A novel methodology to evaluate surface cracking risk during strand straightening in continuous casting

G.Poltarak, S.Ferro, C.Cicutti

A modeling methodology is developed in order to estimate the surface cracking of round bars during straightening in the continuous casting of steel. For this purpose, the termo-mechanical state of the bar is acquired by finite element models, and a material failure criterion is codified afterwards. The output of this methodology is a surface cracking indicator. Hot ductility tests are performed in a Gleeble system to obtain the brittle temperature range of the material. Several cases are modeled, taking into account different bar diameters, casting speeds and steel compositions. These cases are then compared to surface defect measurements performed in a specific steel-shop in order to evaluate the suitability of the model.

KEYWORDS: CONTINUOUS CASTING – CRACKING – MATHEMATICAL MODEL
HOT DUCTILITY – PROCESS VARIABLES

INTRODUCTION

Surface quality in continuous casting products represents a constant challenge in steelmaking research, both in high productivity scenarios and in the manufacturing of high specification materials, since surface cracking can generate defects in the rolled material and even its scrapping. In this article, a methodology is developed whose objective is to estimate the cracking risk in round bars during the straightening in the continuous casting machine. This methodology consists of the thermo-mechanical finite element modeling of the solidifying bar followed by the coding of a failure criterion. First, the heat transfer equations are solved from the meniscus to the billet cut, obtaining the distribution of phase and temperature along the strand. Then, a 3D analysis is carried out using an Eulerian model that provides stress, strain and strain rate distribution. These parameters feed a cracking criterion that calculates the surface cracking risk in the most stretched fiber. Finally, a numerical indicator is obtained in order to quantify how critical the casting conditions are.

The developed methodology is flexible enough to analyze the influence of casting speed changes, bar diameter, steel composition and geometric distribution imposed by pinch-roll units. Model results are compared with statistical data obtained from the surface inspection of final products in a large number of heats. A reasonable agreement between model calculations and defect index in the final product is obtained.

MODELING SEQUENCE

A modeling methodology is developed, consisting of a thermo-mechanical simulation followed by the codification of a surface cracking criterion. A thermal simulation is first carried out using a heat transfer model, which calculates temperature and phase distribution along the bar. Thermal results are then used as an input for the mechanical model, whose main output are strain and strain rate fields. Finally, a surface cracking risk indicator is calculated by the codification of a failure criterion.

HEAT TRANSFER MODEL

Heat transfer problem is solved numerically by an in-house model [1] under the hypothesis that longitudinal heat flow is much lower than the radial flow. Hence, the domain is a travelling transversal section of the casting bar where the 2D heat transfer equation is solved,

$$\frac{d\mathcal{H}}{dT}\frac{\partial T}{\partial t} = \underline{\nabla}\cdot\left(k\underline{\nabla}T\right) + q_v \qquad [1]$$

Guillermo Poltarak,
Sergio Ferro,
Carlos Cicutti
Tenaris R&D Steelmaking, Argentina

where H is the volumetric enthalpy, k the thermal conductivity, and q_v the volumetric heat generation. Eq. 1 has the following boundary conditions:

$T=T_0$ initial bar temperature at the meniscus (liquid steel)
$q\cdot n=q_{mold}$ heat flux imposed at the mold (primary cooling) [2]
$q\cdot n=h(T-T_{bulk})$ convection and radiation to the environment at bar surface

where $q=-k\nabla T$ is the heat flux according to Fourier's Law. Convective heat transfer is used to simulate air and water sprays heat losses, and also to model radiation to the environment, by the application of an effective convection coefficient h which takes into account both effects. Eq. 1 is solved numerically by the finite elements method, using an implicit time integration. Nonlinearities, such as phase changes and parameters dependence with temperature, require the implementation of an iterative algorithm. This thermal model has been applied to optimize casting operative variables [3-4] and was validated with plant measurements [5] taken from different steel-shops.

MECHANICAL MODEL

The mechanical simulation is carried out using a 3D finite element eulerian model [6] which considers the metal as a viscoplastic fluid. Different material states, such as liquid steel, mushy zone, solid material and air are modeled by changing viscosity magnitude along the bar. The mesh is fixed and the free-surface of the material is defined by an auxiliary variable called pseudo-concentration, which is updated through the transport equation. After the free surface is determined, the velocity field at the material has to satisfy the equilibrium equations. The momentum equation leads to the principle of virtual power,

$$\int_V \underline{\underline{\sigma}} : \delta\underline{\underline{\dot{\varepsilon}}}\, dV = \int_V \underline{f}^V \cdot \delta\underline{\dot{u}}\, dV + \int_{S\sigma} \underline{t} \cdot \delta\underline{\dot{u}}\, dS \qquad [2]$$

where V is the material calculation domain, σ is the Cauchy stress tensor, $\dot{\varepsilon}$ the strain rate tensor, f^v the volumetric forces vector, $\dot{u}$ the material velocity vector, $S\sigma$ the domain boundaries, and t the surface forces vector. The model entry section is defined by imposing the initial pseudo-concentration corresponding to the bar diameter, and the casting speed. Rolls are considered as rigid surfaces. As the material cannot penetrate them, the velocity in the direction of the die is imposed as zero. Finally, the exit section is assumed to be completely solid, meaning that the velocity is uniform in that section.

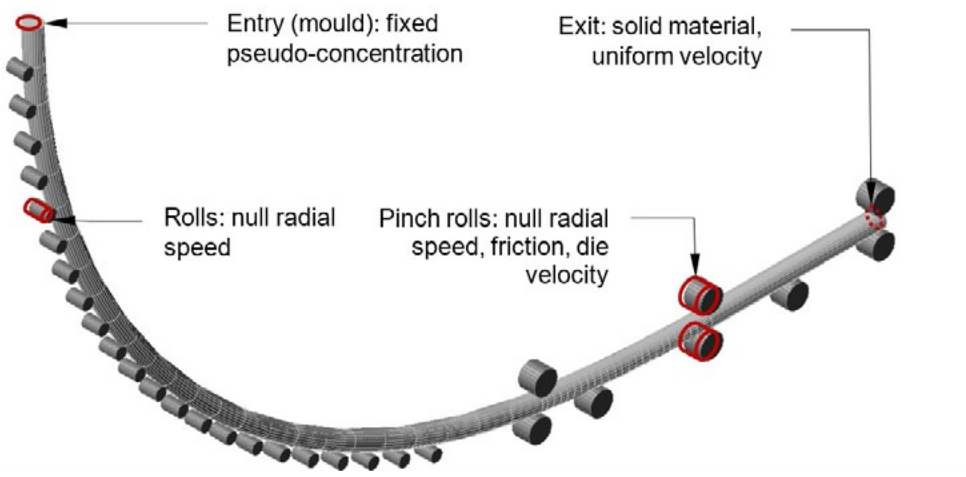

Fig. 1 – Boundary conditions of the mechanical analysis.

Material mechanical behavior is given as a function of temperature, strain and strain rate. A material law developed by Kozlowski et al. [7] is employed in the austenitic range (i.e. when temperature is lower than the corresponding to a 10% content of ferrite, Eq. 3a), and a law proposed by Li and Thomas [8] in the ferritic range (when temperature is higher than the corresponding to a 10% content of ferrite, Eq. 3b).

$$\overline{\sigma}_a = \frac{1}{\sigma_0}\left[\left(\frac{exp(Q/T)}{C}\dot{\overline{\varepsilon}}\right)^{\frac{1}{n}} + a_\varepsilon \overline{\varepsilon}^{n_\varepsilon}\right] \qquad [3a]$$

$$\overline{\sigma}_f = f_C(T/300)^{-5.52}(1+1000\overline{\varepsilon})^m\left(10\dot{\overline{\varepsilon}}\right)^{\frac{1}{n}} \quad [3b]$$

being σ_a and σ_f the equivalent stresses of each phase, σ_0 an initial structure constant, ε the equivalent strain, C and f_C parameters which depend on carbon content, m, n, a_ε and n_ε functions of temperature, Q the activation energy constant, and T the temperature, previously calculated by the thermal model. Phase changes, solidus and liquidus temperatures are extracted from a previously developed segregation model [9] as a function of steel chemical composition. Thermal strains and bar ovalization are analyzed separately and are not included in this study.

SURFACE CRACKING

The predominant cracking mechanisms of solid steel between 700 and 1000 °C is originated by the precipitation of ferrite in the grain boundaries. This softer phase promotes intergranular cracks and is manifested macroscopically as a ductility loss, whose effects are increased by micro-alloys such as niobium and vanadium [10]. Reduction of area tests, at controlled values of temperature and strain rate, are applied to measure this phenomenon.

If the sample undergoes a constriction (smaller final section) the material is ductile and able to absorb a high deformation before fracture. If, however, the final section is similar to the initial, the material is brittle and breaks suddenly. In other words, the critical strain that the material can withstand before breaking is closely related to the reduction of area.

While temperature and strain rate can be kept under control in the laboratory, the situation is different in the mill, since these parameters fluctuate along the bar. Schwerdtfeger [11] developed a failure criterion based on reduction of area trials, which estimates the critical strain that the material is able to resist as,

$$\varepsilon_c = \frac{0.4}{f_{grain} f_{segreg} f_{notch}} \frac{RA}{100} \quad [4b]$$

where f_{grain}, f_{segreg} and f_{notch} are parameters depending on the grain size, solute segregation at grain boundaries and oscillation marks, and RA is the reduction of area at each point. Although Schwerdtfeger proposed an expression to calculate the reduction of area diagram based on several parameters, laboratory tests to evaluate the ductility of specific steel grades were performed. Finally, a "damage integral" that takes into account the cumulative damage at each fiber of the bar is calculated,

$$L_{surf} = \sum_{i=1}^{n} \frac{|\Delta\varepsilon_i|}{\varepsilon_{c\,i}} \quad [5]$$

where i=1,2,…,n represents each time step, $\Delta\varepsilon_i$ is the strain increase at time i, and $\varepsilon_{c\,i}$ is the critical strain the material can withstand at that moment, according to Eq. 4. If L_{surf} exceeds a value of 1, surface cracking is likely to take place.

EXPERIMENTAL PROCEDURE

REDUCTION OF AREA DETERMINATION

Gleeble tests

In order to assess the reduction of area curves of two different steel grades, tension tests were performed in a Gleeble 3500 system. The composition of the tested materials is presented in Table 1. For these tests, 10 mm diameter cylindrical samples were machined from hot rolled material. The samples were heated up to 1330 °C at a rate of 1.5 K/s and held at this temperature for 300 seconds in order to allow grain coarsening and precipitates dissolution. After that, samples were cooled down to testing temperature at a rate of 1.67 K/s, held for 300 seconds for thermal homogenization and deformed until fracture at a strain rate of 10^{-3} s^{-1} in the temperature range of 700 to 1100 °C for both steels. Additional tests were performed at 800 °C for steel B, at strain rates of 10^{-1} and 5 s^{-1}. Both the applied forces and the displacements produced during tests were recorded. Hot ductility was assessed by measuring the reduction of area (RA) of the broken specimens.

Tab. 1 – Chemical composition of tested steels (wt %).

COMPOSITION OF TESTED STEELS						
Steel	C	Mn	Si	V	Nb	Ti
A (no Nb)	0.12	1.05	0.25	0.04	0.00	0.02
B (with Nb)	0.11	0.10	0.25	0.07	0.03	0.00

Curve fitting

A curve fitting of the experimental data was performed in order to get a continuous variation of reduction of area depending on both temperature and strain rate. The variation with strain rate was fitted with a hyperbolic tangent function (Eq. 6, Fig. 2).

$$RA(\dot{\varepsilon}) = 42.8 * \{1 + tanh[0.59 * log(\dot{\varepsilon}) + 1.35]\} \quad [6]$$

The variation with temperature at a fixed strain rate of 10^{-3} s^{-1} was fitted with a scaled beta function [12] for both steels, as shown in Fig. 3, Then, a second scaling was performed using the strain rate formula previously explained (Eq. 6).

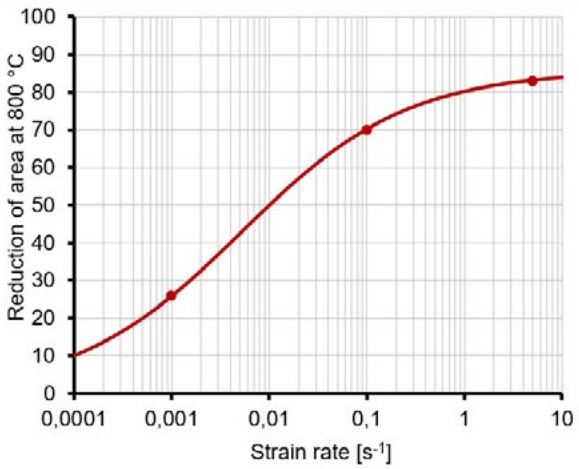

Fig. 2 – Effect of strain rate on the reduction of area at 800 °C.

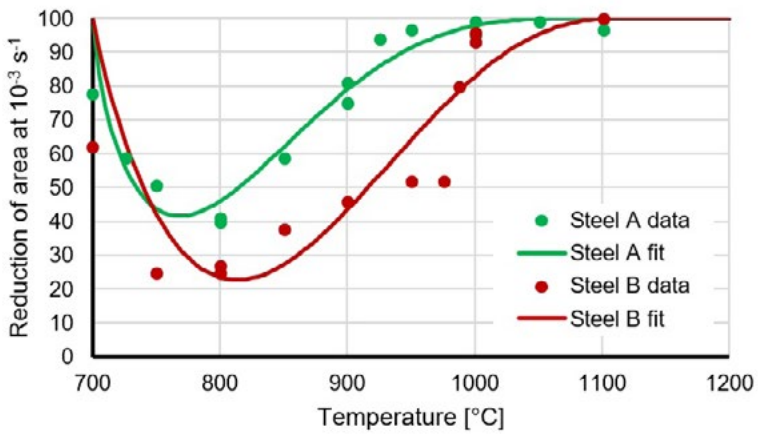

Fig. 3 – Reduction of area at 10^{-3} s^{-1} versus temperature for the two studied steels.

A reduced ductility is observed for both steel grades between 700 and 1100 °C although steel B shows an even more brittle behavior, which can be associated with the Nb precipitates that promote intergranular cracking. The temperature above which the material presents a fully ductile behavior (100% reduction of area) is called T_{db}, taking a value of 1089 °C for steel A and 1112 °C for steel B.

DEFECT INDEX IN ROLLED PRODUCTS

In the plant under analysis, continuous casting round bars are rolled into seamless pipes and the entire production is inspected by Non Destructive Testing (NDT) techniques. Each time an imperfection is detected, it is classified according to a set of pre-established rules. This classification determines the most likely part of the manufacturing process where the imperfection might have been generated (steelmaking, casting, rolling, heat treatment, etc). In the present case, inspection results of more than 5000 heats were compiled. An index to assess the frequency of surface imperfections related to the continuous casting process in each heat was defined. Then, the influence of steel composition and process conditions were evaluated and compared with model predictions.

RESULTS AND DISCUSSION

SURFACE CRACKING RISK CALCULATION

Surface cracking risk is calculated using the procedure explained in Section 1. The analysis is applied to the same caster from which the defectology data is obtained. Modeled calibers cover the entire range of diameters produced in this machine ranging from 148 to 330 mm. A standard casting speed is considered for each caliber, and a speed reduced by 30%, in agreement with the speed defined for the start-up. The two steel grades indicated in Table 1 are evaluated.

At first, bar temperatures are determined with the thermal model depicted in Section 1.1. Surface temperatures are shown in Fig. 4 for all the bar diameters cast at a standard speed as a function of distance to meniscus.

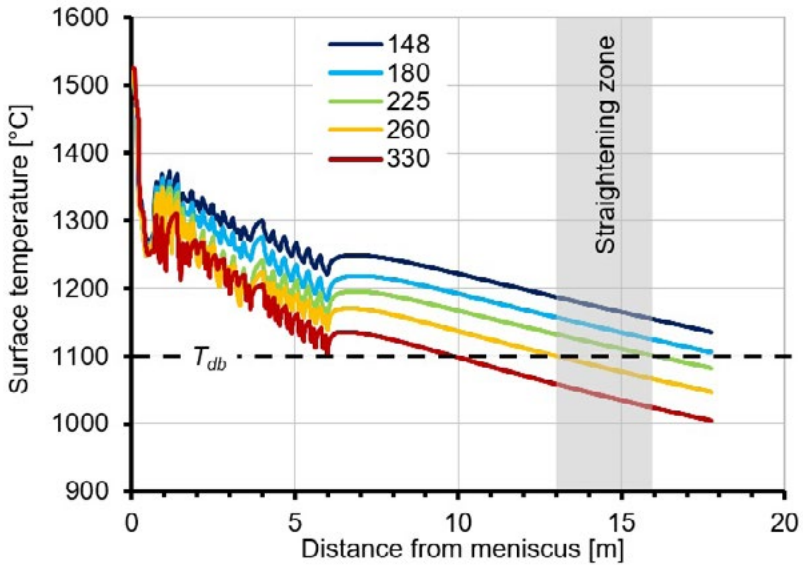

Fig. 4 – Evolution of surface temperature for different bar diameters.

It can be appreciated that the temperatures are lower as the bar diameter increases, since larger sections cast at lower speeds. As seen in Section 2.1, the upper bound of the brittle temperature range T_{db} lies around 1100 °C for the tested steels. If the material is straightened below that temperature, higher cracking risk is expected.

After the thermal simulation, the mechanical model (Section 1.2) is applied to determine stress and strain fields. Surface strain and strain rate along the intrados of the bar (the most stretched fiber) are presented on Fig. 5. Only the 330 mm diameter bar is shown as an illustrative example of the calculation. The strain after each straightening point can be easily compared with the analytical value $\varepsilon_{sn}=(1/R_1-1/R_n)(d/2)$ where ε_{sn} is the accumulated surface strain where the radius changes to R_n, R_1 the first machine radius and d the bar diameter. Analytical estimations of strain rate are fairly rough, thus justifying the use of the model in order to determine this magnitude. Strain rate peaks can be observed in correspondence with the straightening points.

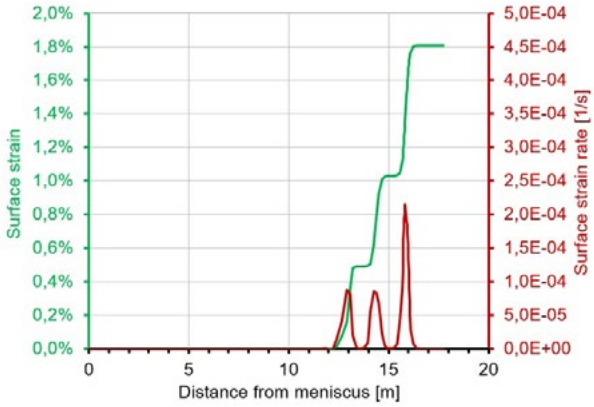

Fig. 5 – Surface strain (green) and strain rate (red) versus distance to steel meniscus.

At last, thermo-mechanical results and ductility tests data are processed together in order to estimate surface cracking risk, as explained in Section 1.3. Reduction of area depends on both temperature (Fig. 4) and strain rate (Fig. 5). In Fig. 6, it can be noticed that the material is straightened with a brittle behavior, since surface temperatures drop below T_{db}. Surface cracking risk is then calculated and its values are also shown in Fig. 6.

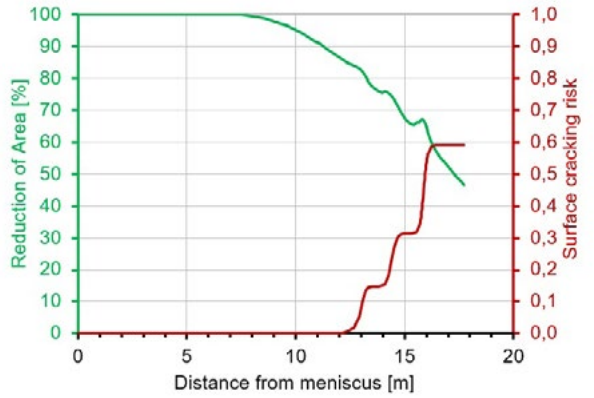

Fig. 6 – Reduction of area (green) and surface cracking risk (red) versus distance from meniscus.

The above procedure is then repeated for all the combinations of diameter, casting speed and steel grade, and the final value of surface cracking risk is obtained for each case. Results are summarized in Fig. 7.

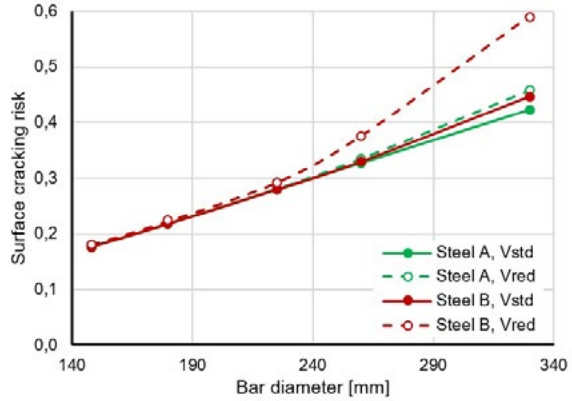

Fig. 7 – Simulation resutls of surface cracking risk as a function of bar diameter, steel composition and casting speed.

A clear cracking risk raise is observed with increasing bar diameters. In small sections, the effects of steel grade and casting speed are negligible. But on larger diameters, Nb alloyed steels present a higher cracking risk. This effect is more evident at reduced casting speed.

CORRELATION BETWEEN MODELED RESULTS AND DEFECT INDEX IN ROLLED MATERIAL

As indicated in Section 2.2, results of pipe inspection in a large number of heats were compiled and analyzed.

At first, the influence of bar diameter and casting sequence were analyzed, as seen in Fig. 8. As the bar size increases, the defect index rises. This trend is in agreement with the results of the model predictions indicated in Fig. 7 and is produced because, in bigger sections, larger strains are generated at the bar surface during unbending.

As the casting speed gradually increases during sequence starts, the first heat of sequence is normally cast at an average lower speed than the rest of the heats. In general, lower casting speeds promote a drop in the strand surface temperature, which can reach T_{db} at the straightening point, increasing the risk of cracking. This fact is verified in the simulations performed, where an increment in the cracking risk is obtained when the casting speed is reduced by 30% (see Fig. 7). So, the larger defect index observed for the first heats of sequence could be partially explained by this effect. It is worth noting that smaller sections are usually cast at higher speeds, so the strand surface temperature remains relatively high during unbending and the effect is less important, as shown in Fig. 7 and 8.

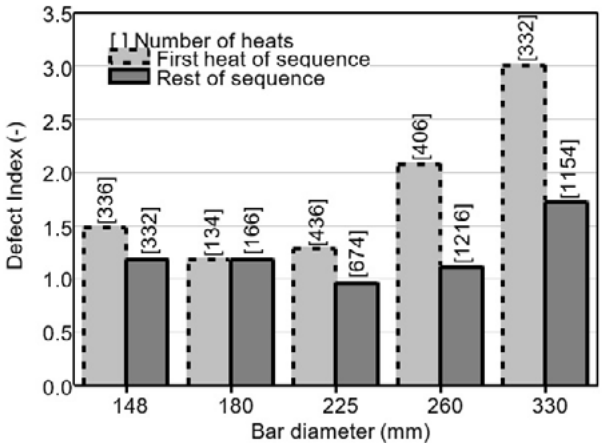

Fig. 8 – Effect of bar diameter and sequence position on defect index. Bar line type is similar than the convention used in Fig. 7: dotted lines represent reduced speed and solid lines stand for standard speed.

In order to study the effect of steel composition on the defect index, two groups of low C steels were formed, one with Nb and the other without Nb. Since steels with Nb are more frequently cast in larger sections, only bars with a diameter greater than 225 mm were considered for this comparison. As indicated in Fig. 9, steels with Nb exhibit a higher defect index, which is in agreement with model predictions shown in Fig. 7.

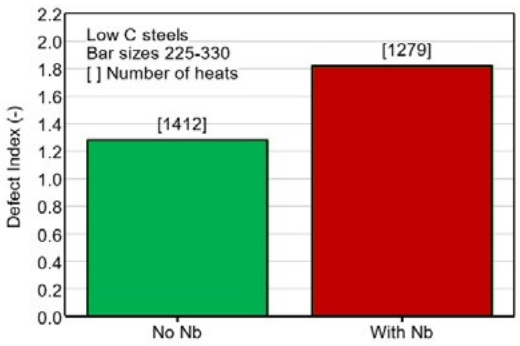

Fig. 9 – Effect of Nb on defect index. Bar colors are chosen according to Fig. 7 since the red bar can be associated with steel A (with Nb) and the green bar with steel B (no Nb).

Finally, the impact of caster type on the defect index was also analyzed. For this analysis, similar steel grades (low C, alloyed with Nb) cast in the same section (330 mm diameter) but in two different continuous casting machines (one vertical and the other curved) were compared. As shown in Fig. 10, the defect index is higher in the material cast in the curved machine, which confirms the role of straightening in the potential formation of defects.

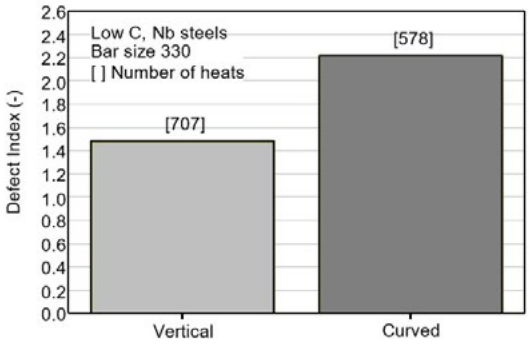

Fig. 10 – Influence of caster type on defect index.

CONCLUSIONS

A thermo-mechanical model was developed, followed by the codification of a material failure criterion to assess the cracking risk of round bars during strand straightening. For the development of the cracking criterion, ad-hoc hot tension laboratory tests were carried out in low carbon steels with and without Nb. Results of these tests showed that the steel alloyed with Nb exhibits a wider and deeper low ductility trough.

The developed methodology was applied to analyze several scenarios. Performed simulations showed that the surface cracking risk is higher as the bar diameter increases, since bigger sections are subject to larger surface strains and lower temperatures at unbending. Both of these effects are detrimental for the material. For similar bar sizes, a reduction in casting speed can increase the risk of cracking because the strand surface temperature decreases and can enter into the low ductility region during straightening. As smaller sections are normally cast at higher speeds, the strand surface temperature remains relatively high during unbending, so the effect is not significant. However, a reduction of casting speed in bigger sections may have a detrimental impact. This effect is even more noticeable when Nb alloyed steels are cast.

Results of industrial inspection of rolled material produced from a large number of heats were carefully analyzed. This evaluation showed that the index of surface defects related to the continuous casting process follows the same trend obtained in the simulated scenarios. Hence, the developed methodology can be used to investigate the role of process variables on the risk of transverse cracking in the continuous casting of round bars.

REFERENCES

[1] Gonzalez M, Goldschmit MB, Assanelli AP, Dvorkin EN, Fernández Berdaguer E. Modeling of the solidification process in a continuous casting installation for steel slabs. Metallurgical and Materials Transactions B, vol. 34, num. 4 (2002), p. 455-473.

[2] Savage J, Pritchard WH. The problem of rupture of the billet in the continuous casting of steel. Journal of the Iron and Steel Institute, vol. 178 (1954), p. 269-277.

[3] Vazquez M, Poltarak G, Ferro S, Campos A, Cicutti C. 8th ECCC, Graz, Austria, Jun-2014.

[4] Ristorto I, Vazquez M, Fuhr F, Alicandro J, Sabugal J, Campos A. 20th IAS Steel Conference, Rosario, Argentina, Nov-2014.

[5] Ferro S, Cardozo M. 5th SteelSim, Ostrava, Czech Republic, Sep-2013.

[6] Dvorkin EN, Toscano RG. A new rigid-viscoplastic model for simulating thermal strain effects in metal forming processes. Int. J. for Numerical Methods in Engineering, num. 58 (2003), p. 1803-1816.

[7] Kozlowski PF, Thomas BG, Azzi JA, Wang H. Simple constitutive equations for steel at high temperature. Metallurgical Transactions A, vol. 23A (1982), p. 903-918.

[8] Li C, Thomas BG. Thermomechanical Finite-Element Model of Shell Behavior in Continuous Casting of Steel. Metallurgical and Materials Transactions B, vol. 35B, num. 6 (2004), p. 1151-1172.

[9] Cicutti C, Boeri R. Analysis of solute distribution during the solidification of low alloyed steels. Steel Research International, vol. 77, num. 3 (2006), p. 194-201.

[10] Maehara Y, Ohmori Y. The Precipitation of AlN and NbC and the Hot Ductility of Low Carbon Steels. Materials Science and Engineering, vol. 62 (1984), p. 109-119.

[11] Schwerdtfeger K, Spitzer KH. Application of Reduction of Area-Temperature Diagrams to the Prediction of Surface Crack Formation in Continuous Casting of Steel. ISIJ International, vol. 49, num. 4 (2009), 512–520.

[12] Hazewinkel M, editor. Encyclopaedia of Mathematics. Springer Netherlands, Hardcover ISBN 978-1556080104 (2001).